Solar Vapor Generation Enabled by Nanoparticles

Oara Neumann,[†] Alexander S. Urban,[†] Jared Day,[†] Surbhi Lal,[†] Peter Nordlander,[†,‡,*] and Naomi J. Halas[†,‡,*]

[†]Department of Electrical and Computer Engineering, [‡]Department of Physics and Astronomy, Laboratory for Nanophotonics, and the Rice Quantum Institute, Rice University, 6100 Main Street, Houston, Texas 77005, United States

ABSTRACT Solar illumination of broadly absorbing metal or carbon nanoparticles dispersed in a liquid produces vapor without the requirement of heating the fluid volume. When particles are dispersed in water at ambient temperature, energy is directed primarily to vaporization of water into steam, with a much smaller fraction resulting in heating of the fluid. Sunlight-illuminated particles can also drive H_2O—ethanol distillation, yielding fractions significantly richer in ethanol content than simple thermal distillation. These phenomena can also enable important compact solar applications such as sterilization of waste and surgical instruments in resource-poor locations.

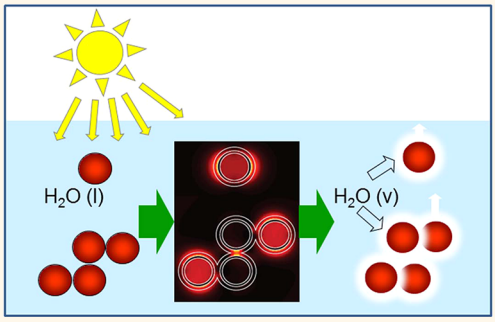

KEYWORDS: plasmon · nanobubble · steam · distillation · photothermal

Solar energy has engendered extraordinary interest for its potential to provide power for a variety of processes without relying on fossil fuels.[1,2] While large-scale solar thermal installations are being developed for electrical power generation, an alternative and currently unmet need is in compact solar energy sources that drive vital processes directly, in addition to the generation of electrical power. These types of smaller scale, stand-alone solar energy converters could directly enable a range of applications, both in first-world countries and in the developing world. Light-to-heat conversion by conductive nanoparticles, under laser illumination, has been shown to induce dramatic localized heating and even vaporization of their host medium.[3−15] Here we show that this process can be used for solar-based direct steam generation, without the requirement of heating the liquid volume to the boiling point. Submicrometer particles that can absorb light across the solar spectrum produce steam in a matter of seconds when dispersed in water and can achieve steam temperatures well above 100 °C in compact geometries. With particles dispersed in an ethanol−water mixture, solar distillation yields a distillate substantially richer in ethanol than what would be obtained using a conventional heat source. Under these unusual nonequilibrium conditions, the water−ethanol azeotrope is breached and ethanol fractions approaching 99% are straightforwardly obtained.

Subwavelength metallic particles are intense absorbers of optical radiation, due to the collective oscillations of their delocalized conduction electrons, known as surface plasmons. When excited on resonance, energy not reradiated through light scattering is dissipated through Landau (nonradiative) damping,[16] resulting in a dramatic rise in temperature in the nanometer-scale vicinity of the particle surface. This heat generation process has been of great interest for applications, for example, in biomedicine, where photothermal cancer therapy,[17] laser-induced drug release,[18] and nanoparticle-enhanced bioimaging[19] all rely on this property. Carbon-based particles have also been shown to give rise to very strong photothermal heating effects.[20,21] Particle-based approaches have also been of interest for solar energy applications;[22,23] however, such studies have focused primarily on improving the thermal conductivity of working fluids and have not addressed the energy advantage of directly capturing the latent heat of vaporization required for liquid−vapor phase transitions.

Light-absorbing nanoparticles, when appropriately illuminated,[3,24−26] can reach temperatures well above the boiling point

* Address correspondence to halas@rice.edu, nordland@rice.edu.

Received for review October 24, 2012 and accepted November 18, 2012.

Published online November 19, 2012
10.1021/nn304948h

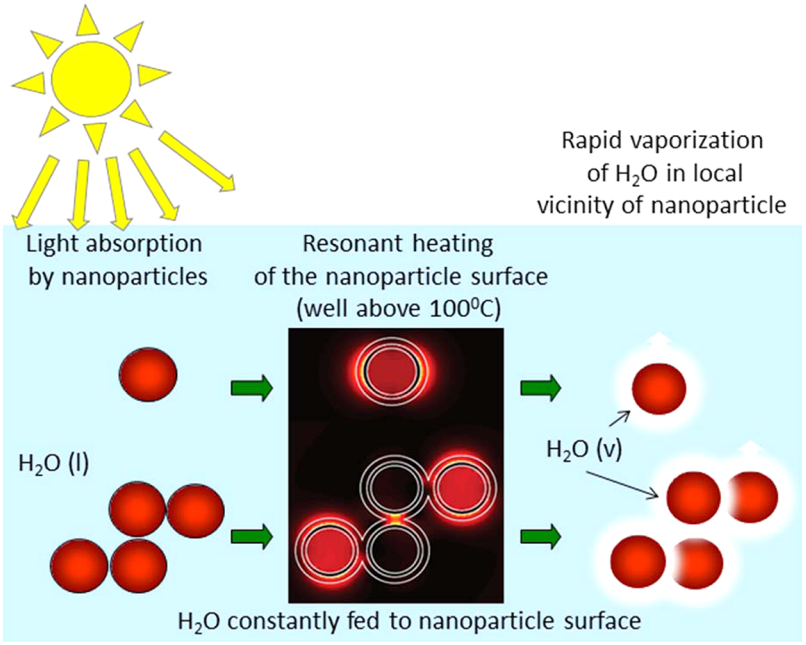

Figure 1. Schematic of nanoparticle-enabled solar steam generation: initially, light is absorbed by nanoparticles, raising their surface temperature above the boiling point of the fluid. The nanoparticle surface serves as a boiling nucleation site. Vapor is formed around the nanoparticle surface, and the complex moves to the liquid–air interface, where the steam is released. New liquid is replenished at the hot nanoparticle surface, and the process is repeated.

of liquid water,[3] creating a nonequilibrium condition between the hot nanoparticle surface and the cooler fluid (Figure 1).[27,28] Once vapor is formed at the particle–liquid interface, the metallic nanoparticle is enveloped in a thin layer of steam with a reduced thermal conductance compared to the liquid. Under continued illumination, the vapor volume increases, may possibly coalesce with other nanobubble complexes, and eventually moves to the liquid–air interface, where the vapor is released and the nanoparticles revert back to the solution to repeat the vaporization process. While steam is produced virtually instantaneously and quite vigorously, even explosively, depending on illumination geometry, the nanoparticles remain in the fluid volume and are not conveyed into the vapor phase. As the nanoparticles move to the liquid–vapor interface, they exchange heat with the fluid, slightly raising the fluid temperature. During prolonged periods of illumination, the bulk temperature of the liquid gradually increases, ultimately resulting in conventional boiling of the fluid volume as a parallel effect. However, because there is no need to heat the fluid, the process is intrinsically more efficient than any vapor-producing method that requires volume heating of the fluid in macroscopic quantities, such as conventional thermal sources.

RESULTS AND DISCUSSION

Solar Steam Generation Experiments. To quantify the particle-nucleated solar steam generation process, two solutions of absorbing nanoparticles, (i) SiO_2/Au nanoshells and (ii) water-soluble N115 carbon nanoparticles,[21] with equivalent integrated optical densities (from 400 to 1300 nm in wavelength), were prepared (see Supporting Information). Each solution was placed in its own transparent tube, where a small thermocouple was inserted into the fluid volume far from the region of optical illumination. The tube was then partially immersed in an ice bath, except for the region of the tube that was illuminated (see Supporting Information). As the tube was illuminated, the steam pressure and the temperature of the fluid volume were monitored (Figure 2). Upon solar illumination, the pressure over the solution of nanoshells began to increase, indicating steam generation, less than 5 s after illumination commenced (at t = 0), while for carbon nanoparticles the pressure increase was delayed by just over 20 s. Once started, however, the steam is generated at a very similar rate for both solutions. Steam generation from the metallic nanoparticle solution occurred in small, microexplosive "bursts", which can be seen in the relatively noisier pressure increase for these nanoparticles. Although both suspensions of particles show a similar increase in the rate of steam generation with time, there is a dramatic difference between the temperature of the fluid volume during illumination for the carbon nanoparticle and for the nanoshell solution over this initial time period (Figure 2B). We observe a slow and measurable increase in the fluid temperature for the illuminated nanoshell solution, while the carbon nanoparticle solution shows only a negligible increase in temperature for the same illumination conditions during this initial time period. The observed fluid heating is due to heat transfer into the solution from the nanoparticle–bubble

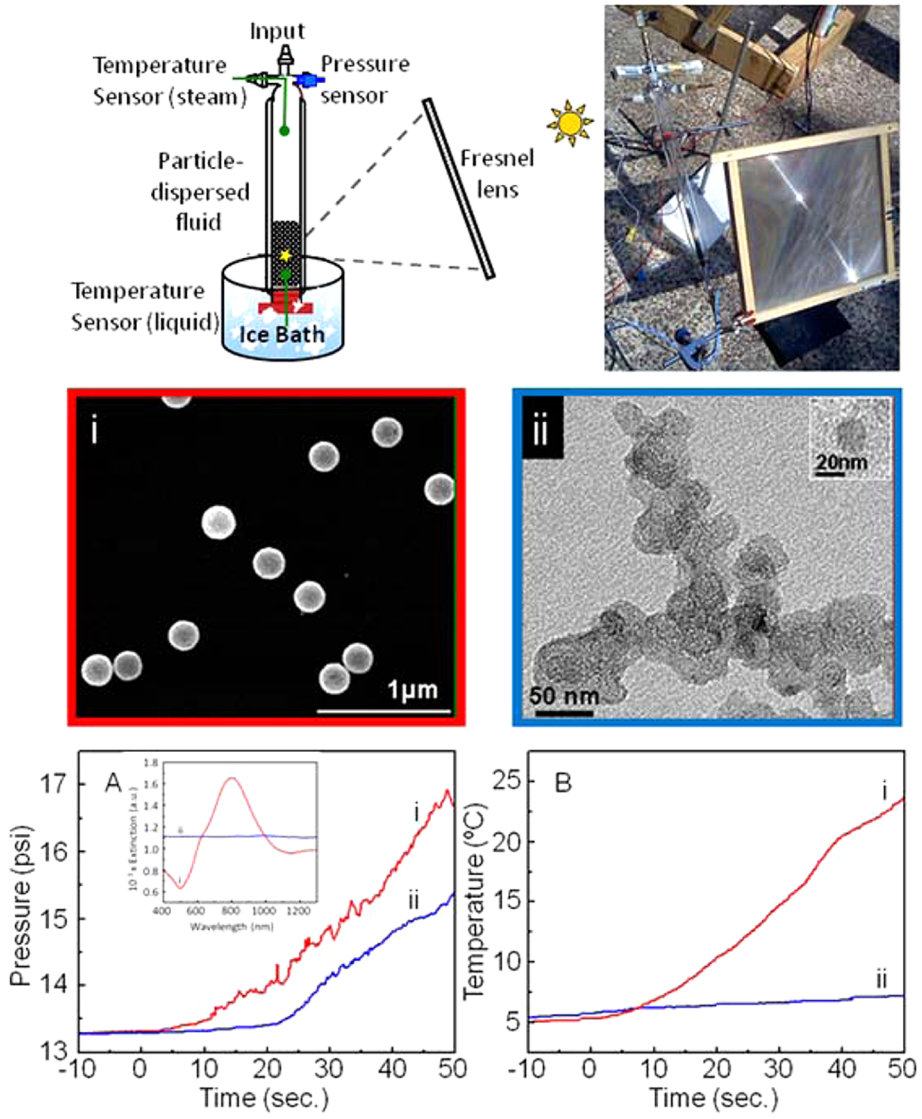

Figure 2. Pressure−temperature evolution with time of solar steam generation in ice bath conditions: (A) Pressure *vs* time and (B) temperature *vs* time for (i) SiO_2/Au nanoshells dispersed in water and (ii) carbon particles N115 dispersed in water under solar exposure, measured in a transparent vessel isolated with a vacuum jacket to reduce thermal losses and with a solid copper base for enhanced thermal conductivity. Inset: UV−vis spectra of Au nanoshells (red) and carbon particles (blue). The vessel was illuminated with solar radiation focused by a 26.67 cm × 26.67 cm Fresnel lens with a 44.5 cm focal length, while the nanoparticle solution was immersed in an ice bath. The optical density was equivalent for both particle solutions.

complexes, an effect that is most probably linear in nanoparticle concentration generally, but concentration independent in this optically dense regime. The difference in the initial increase in fluid temperature between the two types of nanoparticles is most likely due to the metallic nanoparticles heating more rapidly than the carbon nanoparticles. The carbon nanoparticles initially lose less energy to the surrounding solution than the metallic nanoparticles, quite possibly due to their greater buoyancy during the steam generation process. When this experiment is performed without an ice bath, the secondary fluid heating seen in the case of metallic nanoparticles leads ultimately to conventional boiling in addition to particle-induced steam generation. Under these conditions, elevated steam temperatures (140 °C) are observed within a ten-minute irradiation time. Analysis of the volatile and condensed vapor showed no evidence of chemical modification.

To quantify the energy efficiency of solar steam generation, an open volume with an aqueous solution of particles was irradiated using focused sunlight for a ten-minute duration, while both the mass loss due to steam generation and the temperature increase due to heating of the liquid were simultaneously monitored (Figure 3). We examined solutions of nanoshells and carbon nanoparticles with equal optical densities and different solution volumes (25 and 35 mL). Following the initial "turn-on" period, constant rates of mass loss and fluid heating, the latter dependent upon the fluid volume, were observed (Figure 3a, b). These constant rates allow us to assume that additional loss mechanisms are minimal and, therefore, quantify the relative amount of solar energy used in the

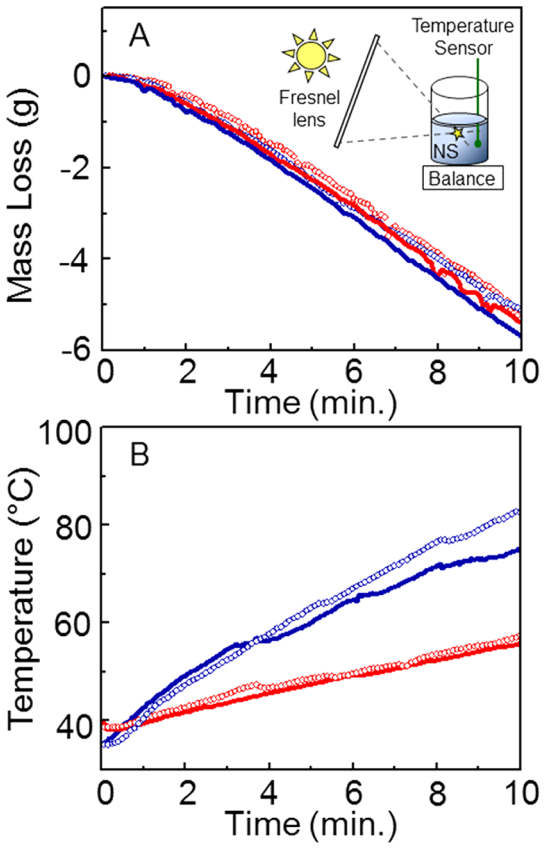

Figure 3. Measurements of mass loss due to steam generation and heating of the fluid volume during solar irradiation of particle suspensions. (A) Mass loss and (B) temperature increase of solution for two different solution volumes, 25 mL (blue) and 35 mL (red), for nanoshell solution (solid dots) and (open dots) carbon particles. Inset of (A) illustrates the experiment schematically.

steam generation process and that used to heat the fluid. For constant incident solar power, the temperature increases for both fluid volumes correspond to a 5 W consumption of power: however, the rate of energy consumption by steam generation, as determined by mass loss, is 23.5 W (see Supporting Information for analysis). These measurements indicate that 82% of the solar energy absorbed by the nanoparticles contributes directly to steam generation.

Theoretical Analysis. The steam generation in this present experiment is a dramatic nonequilibrium process. A bubble without an encapsulated heat-generating nanoparticle has no chance of escaping the liquid, but instead would collapse within milliseconds. In the following, we analyze the heat generation around a gold nanoshell of the same dimensions as those used in the experiment. A calculation using the conventional macroscopic model for nanoparticle-induced heating of a surrounding liquid[3] yields a negligible heating of the surrounding water. In the conventional approach, the temperature of the nanoparticle is estimated using the heat transfer equation:

$$\rho(\vec{r})\, c(\vec{r}, t)\frac{\partial T(\vec{r}, t)}{\partial t} = \nabla\cdot[k(\vec{r}, t)\, \nabla T(\vec{r}, t)] + P(\vec{r}, t)$$

Considering the time scales on which the processes involved here occur, the time dependence of the thermal conduction and heat capacity due to convection are negligible, and the equation can be solved analytically in the steady-state regime, yielding a maximum temperature located at the surface of the nanoparticle:[3]

$$\Delta T(R_{NP}) = \frac{V_{NP} P_{abs}}{4\pi k_0 R_{NP}}$$

where R_{NP} = 85 nm and $V_{NP} \approx 2.57 \times 10^6$ nm^3 are the radius and volume of the nanoparticles, k_0 = 0.6062 W/(m K)[29] is the thermal conductivity of the surrounding liquid, and P_{abs} is the local light induced heating of the nanoparticle, which in the present experiment is equal to 9.93×10^{12} W/m^3. Using these parameters, the conventional model predicts a steady-state temperature increase of the surrounding water of only ΔT_{water} = 0.04 °C. With such a modest heat increase, no bubble formation can occur, in drastic disagreement with the steam generation clearly observed in our experiment.

While there is no physical reason to expect that a macroscopic heat transfer model would be appropriate in realistic nonequilibrium nanoscale systems, it is interesting to speculate on why the conventional model fails. The most problematic assumption with this model is the neglect of the interfacial thermal resistance between the nanoparticle and the surrounding water. Interfaces present obstacles to heat flow, creating thermal barriers.

There are many possible mechanisms that could introduce thermal barriers, particularly at the nanoscale. One example is the Kapitza resistance for vibrational energy transfer,[30] which here can be induced through the surface potential induced shifts of the vibrational energies of water molecules adsorbed on the gold surface compared to water molecules in bulk. An energy mismatch of the vibrational modes of two nearby molecules prevents energy transfer. In the present situation the mismatch of the vibrational energies of a layer of water molecules next to the nanoparticle and a layer further away would limit the energy transfer between these two layers and thus from the nanoparticle into the surrounding water. Another possible mechanism that could introduce a thermal barrier could be thermal desorption of adsorbed water molecules because of the nanoparticle heating. A spatial separation between the water molecules and the surface of the gold nanoparticle would result in an immediate loss of thermal contact, greatly reducing the heat transfer into the surrounding water.

It is interesting to note that the conventional model described above predicts a monotonically increasing temperature with decreasing thermal conductance, k_0. Thus for a sufficiently large thermal barrier, arbitrary large temperature increases would result even in the conventional model. Once a bubble has formed around the nanoparticle, the conventional model,

which assumes direct contact between the nanoparticle and the surrounding liquid, clearly fails because the thermal conductance of water vapor is significantly smaller than that of water. If the dimension of the initially formed nanobubble is smaller than the mean free path of the water molecules, the thermal conductance will be even lower than what it would be for a macroscopic gas in equilibrium. While realistic modeling of heat transfer across the water layer is likely to be quite complex—beyond the naïve classical model, and instead requiring a rigorous, atomistic molecular dynamics approach—this task lies beyond the scope of the present paper. Here we show that the observed bubble formation and steam generation do not violate energy conservation and can, just as observed, give rise to large water vapor bubbles.

The experiments show that bubble and steam generation occurs after nominally t_{abs} =10 s of illumination. With the solar illumination intensity used in the experiment, a total energy of $Q_{abs} = t_{abs} \times P_{abs} = 1.7 \times 10^{-7}$ J is absorbed by a single nanoparticle (Figure 4A). This is an enormous energy at the nanoscale. If none of this energy is dissipated into the surrounding water, the temperature of the nanoparticle would increase by 4.37×10^{7} K. Since the experiment does not show any evidence of nanoparticle melting, it is clear that most of this energy is dissipated into the surrounding water. However, the experiment clearly reveals that this energy is not squandered by heating the liquid, but results instead in the generation of water vapor.

In the presence of a thermal barrier at the nanoparticle interface, the induced local temperature can be very large. We now make the simple assumption that the energy absorbed by the nanoparticle is partitioned between the metal and water vapor in a surrounding bubble, which for simplicity is assumed thermally isolated from the surrounding water. This assumption can be justified from the experimentally observed effect: bubbles and steam appear after just a few seconds, without appreciable bulk heating of the surrounding fluid.

The observed steam temperature is approximately 150 °C. The internal pressure within the bubble is almost certainly larger than the ambient pressure of 1 atm due to surface tension, in particular for small bubbles. For simplicity, we assume an internal pressure of 2 atm. The creation of water vapor from liquid water at 25 °C requires an energy of $q_{vapor} = 3.06 \times 10^{-21}$ J/nm^3. The heating of the nanoparticle from 25 to 150 °C costs an energy of $Q_{NP} = 7.30 \times 10^{-13}$ J. In this model the radius R of the bubble can then be estimated from

$$\frac{4}{3}\pi(R_{bubble}{}^3 - R_{NP}{}^3)q_{vapor} + Q_{NP} = Q_{abs}$$

giving $R_{bubble} = 27.1$ μm. This simple estimate is based on rudimentary approximations, but most importantly shows that macroscopic bubble formation around

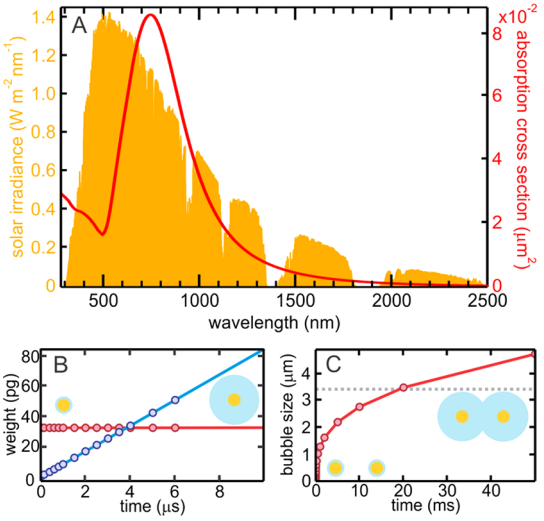

Figure 4. Steam bubble formation through solar absorption by gold nanoshells. (a) The absorption cross section of the gold nanoshells is tuned to overlap the solar spectral irradiance (AM 1.5 G). (b) Comparison of the combined weight of a gold nanoshell and its surrounding steam bubble (red curve) with the weight of the displaced water (blue curve) over time. After 4 μs, the density of the encapsulated nanoshell becomes less than that of the surrounding water, causing the nanoshell to rise to the surface, releasing the steam bubble. (c) Size of the steam bubble surrounding a nanoshell over time (red curve). After 20 ms of steam generation, the size of the bubbles becomes larger than half the average distance between the nanoshells (horizontal gray line), allowing the bubbles to coalesce, thus further enhancing the steam generation process.

nanoparticles indeed is energetically possible. We note that the total mass of such a bubble including the nanoparticle is 9.54×10^{-11} g, which is smaller than the mass of the displaced water by 3 orders of magnitude. Such a bubble with its encapsulated nanoparticle is therefore expected to rise to the surface of the liquid, where the steam will be released, with the nanoparticle subsequently sinking back into the liquid. On the basis of this picture, we plot the increase in weight of the bubble−nanoparticle complex *versus* the weight of the displaced water, for the incident solar power in our experiment (Figure 4B). Here we see that after just 4 μs, the nanoparticle-generated bubble is capable of buoyancy. Also, for the concentrations used in the experiment, the average nanoparticle separation in the liquid is 6 μm. With the present solar intensity, bubbles with their encapsulated nanoparticles are expected to be large enough to coalesce into neighboring nanoparticle-generated bubbles after just 20 ms (Figure 4C). For the case of two identical nanoparticle−bubble complexes, coalescence will double the volume of the vapor and double the heat absorption while only increasing the radius by a factor of $2^{1/3}$ and the surface area of the bubble by $4^{1/3}$. Since the heat transfer from the vapor into the surrounding liquid is proportional to the area of the vapor liquid interface, coalescence of bubbles reduces the heat transfer into the surrounding liquid.

While a more refined model is clearly needed, the observed effect introduces a multitude of legitimate questions and casts serious doubt on the appropriateness of the conventional macroscopic model as an apt description of nanoscale heat flow in this context. This is a very important conclusion, because until now, the conventional macroscopic model has been the accepted canon by the vast majority of researchers in this field. As the bubble grows, energetic gas phase water molecules fueled by the hot nanoparticle surface will also sputter water molecules from the interior of the bubble–water interface, transferring some of their kinetic energy to the liquid. The kinetic distribution of water molecules inside the bubble is likely to be far from local thermal equilibrium. Optically induced electronic effects, such as intense local field enhancements or even optically excited electrons, may lead to the initial formation of a thin vapor around the nanoparticle. Once a thin bubble is formed, heat cannot transfer directly into the surrounding liquid, but instead must pass through the vapor layer with its much lower thermal conductivity. The coalescence of bubbles with their encapsulated nanoparticles may also play a crucial role in steam generation. Because the buoyancy of the encapsulated nanoparticles as calculated previously is large enough to bring the bubble complex to the surface of the liquid, the coalescence of bubbles is probably not essential for the release of the vapor shell. However, it may greatly reduce the heat loss of the nanoparticle–bubble complex into the liquid, thereby increasing the efficiency of solar steam generation.

Distillation. Nanoparticle-enabled vaporization can also be applied to the separation of liquids, for a solar-based distillation process with distillate fractions significantly richer in the more volatile component than the case of distillation using a conventional thermal heat source (Figure 5). We distilled ethanol–water mixtures (20 mL) with Au nanoshell particle dispersants (2.5×10^{10} particles/mL) using focused sunlight (a 26.67 cm $\times$ 26.67 cm area Fresnel lens with a 44.5 cm focal length). The mixtures were initially contained in a 100 mL vessel with a vacuum jacket to prevent heat loss. Vapors generated by solar illumination were cooled by a simple water-cooled condenser (Figure 5A), and 10 drops of each distillate fraction were collected. The distillation samples were diluted (1/1000 in water) and analyzed by gas chromatography (GC) on a Hewlett-Packard 5890 GC equipped with a glass column containing 80/120 Carbopack B-DA*/4% Carbowax 20 M (Supelco, Bellefonte, PA, USA) and a flame-ionization detector (Agilent Technologies). A 5 μL sample of the diluted distillate was injected into the GC unit, and the heating program was set to 250, 110, and 250 °C for the injector, oven, and detector, respectively. Identification and quantification were performed using a calibration curve with ethanol

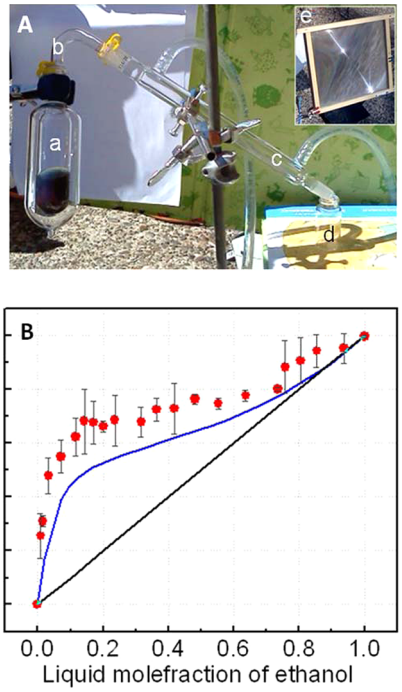

Figure 5. Solar distillation of ethanol. (A) Photo of the solar distillation apparatus including (a) vacuum-jacketed glass container, (b) connector tube, (c) water condenser, and (d) fraction collector vessel. The solution was irradiated by a (e) 26.67 $\times$ 26.67 cm Fresnel lens with a 44.5 cm focal length (inset). (B) Vapor–liquid diagram of ethanol–water fractions produced by solar distillation. Mole % of ethanol in vapor phase for Au nanoshell alcohol–water mixtures under solar exposure (red dots) and standard equilibrium distillation curve at 1 atm and 25 °C (blue curve). The Au nanoshell concentration is 2.5×10^{10} particles/mL.

standards prepared by diluting 200-proof ethanol with MQ water (see Supporting Information). The vapor–liquid phase diagram of ethanol and water produced by solar distillation, relative to a standard equilibrium distillation curve at 1 atm and 25 °C, is shown in Figure 5B. The mole % ethanol obtained in the distillate is consistently higher than that obtained by conventional flash distillation, most likely because the hot surfaces of the illuminated nanoparticles induce preferential vaporization of the more volatile component of the mixture. Analysis of the distillate showed no presence of particles in the distillate nor any evidence of methanol, acetic acid, or other molecules that would result from chemical degradation of the ethanol. Regions of larger and smaller error bars reflect concentration ranges where qualitatively different behavior of the ethanol–water mixture was observed. For example, from 10% to 45% ethanol mole fraction, particle-based steam generation results in turbulent fluid behavior, while from 45% to 75% ethanol mole fraction, particle-based steam generation occurs with virtually no turbulence, under identical illumination conditions. The larger error bars in the regime of >75% ethanol mole fraction are due to the high levels of humidity in the air ambient. For this reason it is quite likely that the

distillates are even higher in ethanol content than the measured averages plotted in the figure. The unusual behavior in these regimes and the effects of ambient humidity are being addressed in ongoing studies using conventional laser sources in nitrogen-purged environments.

The overall energy efficiency of the steam generation process in this unoptimized experimental geometry is 24% (see Supporting Information), which could be improved by minimizing losses, such as improving the collection optics by using reflectors. These results clearly indicate that solar steam generation is a process that has significant potential for use in a wide variety of energy- and sustainability-relevant applications. Solar-driven, stand-alone waste processing or water purification systems could be developed based on this process. High-temperature (~115 °C and above) steam produced directly using sunlight could also be used for compact sterilization or sanitation purposes, from the processing of medical waste to the cleaning of medical or dental equipment, minimizing the resource, time, and input chemical requirements demanded by current methods. With further development, this approach may be adaptable to higher pressures and other working fluids to drive turbines in solar energy harvesting applications. This approach may also be modified to harvest radiant energy from sources other than the sun, for instance, for the capture of waste energy from geothermal, residential, or biological sources.

CONCLUSION

Using absorptive nanoparticles dispersed in water, we demonstrate efficient direct steam generation using solar illumination. A thermodynamic analysis shows that 80% of the absorbed sunlight is converted into water vapor and only 20% of the absorbed light energy is converted into heating of the surrounding liquid. In an application to ethanol distillation, we show that the distillate contains a higher percentage of ethanol than what is predicted by the water–ethanol azeotrope. These findings cast doubts on the conventional macroscopic models for thermal transport between nanoparticles and their environment and suggest that significant thermal barriers may be present at the nanoparticle liquid–vapor bubble interfaces. Most importantly, our findings open up a wide range of novel compact solar energy applications such as distillation, desalination, and sterilization and sanitation applications in resource-poor locations.

METHODS

Fabrication and Characterization of Particles. Carbon black N115 particles were purchased from Cabot, Inc. (Billerica, MA, USA). SiO_2 core–Au shell nanoshells were fabricated as previously described.[31,32] Briefly, 120 nm diameter silica nanoparticles obtained from Precision Colloids, Inc. were suspended in ethanol. The particle surface was then functionalized with 3-aminopropyltriethoxysilane (Gelest). A very small gold colloid (1–3 nm diameter) was grown via the method of Duff *et al.*[33] This colloid was aged for 4–14 days at 6–8 °C. The functionalized silica particles were then added to the gold colloid suspension. The gold colloid adsorbs to the amine groups on the silica surface, resulting in a silica nanoparticle covered with islands of gold colloid called the seed. Au/SiO_2 nanoshells were then grown by reacting $HAuCl_4$ (Sigma-Aldrich) with the seeds in the presence of formaldehyde.

Conflict of Interest: The authors declare no competing financial interest.

Acknowledgment. We gratefully acknowledge the Robert A. Welch Foundation (C-1220 and C-1222) and the Bill and Melinda Gates Foundation for financial support. We thank Joseph Young and Bruce Brinson for technical support and Lisa V. Brown and Tumasang Nche Fofang for helpful discussions.

Supporting Information Available: Details of experimental analysis and gas chromatography data for the solar distillation are provided. This material is available free of charge *via* the Internet at http://pubs.acs.org.

REFERENCES AND NOTES

1. Luzzi, A.; Lovegrove, K. Solar Thermal Power Generation. *Encyclopedia of Energy*; Elsevier Inc., 2004; Vol. 5, pp 669–683.
2. Meier, A.; Gremaud, N.; Steinfeld, A. Economic Evaluation of the Industrial Solar Production of Lime. *Energy Convers. Manage.* **2005**, *46*, 905–926.
3. Govorov, A. O.; Richardson, H. H. Generating Heat with Metal Nanoparticles. *Nano Today* **2007**, *2*, 30–38.
4. Hirsch, L. R.; Stafford, R. J.; Bankson, J. A.; Sershen, S. R.; Rivera, B.; Price, R. E.; Hazle, J. D.; Halas, N. J.; West, J. L. Nanoshell-Mediated Near-Infrared Thermal Therapy of Tumors Under Magnetic Resonance Guidance. *Proc. Natl. Acad. Sci. U. S. A.* **2003**, *100*, 13549–13554.
5. Lukianova-Hleb, E.; Hu, Y.; Latterini, L.; Tarpani, L.; Lee, S.; Drezek, R. A.; Hafner, J. H.; Lapotko, D. O. Plasmonic Nanobubbles as Transient Vapor Nanobubbles Generated around Plasmonic Nanoparticles. *ACS Nano* **2010**, *4*, 2109–2123.
6. Chen, X.; Chen, Y. T.; Yan, M.; Qiu, M. Nanosecond Photothermal Effects in Plasmonic Nanostructures. *ACS Nano* **2012**, *6*, 2550–2557.
7. Carlson, M. T.; Green, A. J.; Richardson, H. H. Superheating Water by CW Excitation of Gold Nanodots. *Nano Lett.* **2012**, *12*, 1534–1537.
8. Baffou, G.; Bon, P.; Savatier, J.; Polleux, J.; Zhu, M.; Merlin, M.; Rigneault, H.; Monneret, S. Thermal Imaging of Nanostructures by Quantitative Optical Phase Analysis. *ACS Nano* **2012**, *6*, 2452–2458.
9. Donner, J. S.; Baffou, G.; McCloskey, D.; Quidant, R. Plasmon-Assisted Optofluidics. *ACS Nano* **2011**, *5*, 5457–5462.
10. Ye, E. Y.; Win, K. Y.; Tan, H. R.; Lin, M.; Teng, C. P.; Mlayah, A.; Han, M. Y. Plasmonic Gold Nanocrosses with Multidirectional Excitation and Strong Photothermal Effect. *J. Am. Chem. Soc.* **2011**, *133*, 8506–8509.
11. Liu, Z. W.; Hung, W. H.; Aykol, M.; Valley, D.; Cronin, S. B. Optical Manipulation of Plasmonic Nanoparticles, Bubble Formation and Patterning of SERS Aggregates. *Nanotechnology* **2010**, 21.

12. Ma, H. Y.; Bendix, P. M.; Oddershede, L. B. Large-Scale Orientation Dependent Heating from a Single Irradiated Gold Nanorod. *Nano Lett.* **2012**, *12*, 3954–3960.
13. Baffou, G.; Quidant, R.; de Abajo, F. J. G. Nanoscale Control of Optical Heating in Complex Plasmonic Systems. *ACS Nano* **2010**, *4*, 709–716.
14. Sanchot, A.; Baffou, G.; Marty, R.; Arbouet, A.; Quidant, R.; Girard, C.; Dujardin, E. Plasmonic Nanoparticle Networks for Light and Heat Concentration. *ACS Nano* **2012**, *6*, 3434–3440.
15. Zhu, M.; Baffou, G.; Meyerbroker, N.; Polleux, J. Micropatterning Thermoplastic Gold nanoarrays to Manipulate Cell Adhesion. *ACS Nano* **2012**, *6*, 7227–7233.
16. Gao, Y.; Yuan, Z.; Gao, S. W. Semiclassical Approach to Plasmon-Electron Coupling and Landau Damping of Surface Plasmons. *J. Chem. Phys.* **2011**, 134.
17. Lal, S.; Clare, S. E.; Halas, N. J. Nanoshell-Enabled Photothermal Cancer Therapy: Impending Clinical Impact. *Acc. Chem. Res.* **2008**, *41*, 1842–1851.
18. Skirtach, A. G.; Dejugnat, C.; Braun, D.; Susha, A. S.; Rogach, A. L.; Parak, W. J.; Mohwald, H.; Sukhorukov, G. B. The Role of Metal Nanoparticles in Remote Release of Encapsulated Materials. *Nano Lett.* **2005**, *5*, 1371–1377.
19. Boyer, D.; Tamarat, P.; Maali, A.; Lounis, B.; Orrit, M. Photothermal Imaging of Nanometer-Sized Metal Particles among Scatterers. *Science* **2002**, *297*, 1160–1163.
20. Moon, H. K.; Lee, S. H.; Choi, H. C. *In Vivo* Near-Infrared Mediated Tumor Destruction by Photothermal Effect of Carbon Nanotubes. *ACS Nano* **2009**, *3*, 3707–3713.
21. Han, D. X.; Meng, Z. G.; Wu, D. X.; Zhang, C. Y.; Zhu, H. T. Thermal Properties of Carbon Black Aqueous Nanofluids for Solar Absorption. *Nanoscale Res. Lett.* **2011**, *6*.
22. Otanicar, T. P.; Phelan, P. E.; Golden, J. S. Optical Properties of Liquids for Direct Absorption Solar Thermal Energy Systems. *Solar Energy* **2009**, *83*, 969–977.
23. Otanicar, T. P.; Phelan, P. E.; Prasher, R. S.; Rosengarten, G.; Taylor, R. A. Nanofluid-Based Direct Absorption Solar Collector. *J. Renewable Sustainable Energy* **2010**, *2*, 033102–13.
24. Richardson, H. H.; Hickman, Z. N.; Govorov, A. O.; Thomas, A. C.; Zhang, W.; Kordesch, M. E., Thermooptical Properties of Gold Nanoparticles Embedded in Ice: Characterization of Heat Generation and Melting. *Nano Lett.* **2006**, *6*, 783−788.
25. Roper, D. K.; Ahn, W.; Hoepfner, M. Microscale Heat Transfer Transduced by Surface Plasmon Resonant Gold Nanoparticles. *J. Phys. Chem. C Nanomater. Interfaces* **2007**, *111*, 3636–3641.
26. Adleman, J. R.; Boyd, D. A.; Goodwin, D. G.; Psaltis, D. Heterogenous Catalysis Mediated by Plasmon Heating. *Nano Lett.* **2009**, *9*, 4417–4423.
27. Huttmann, G.; Birngruber, R. On the Possibility of High-Precision Photothermal Microeffects and the Measurement of Fast Thermal Denaturation of Proteins. *IEEE J. Sel. Top. Quantum Electron.* **1999**, *5*, 954–962.
28. Lapotko, D. Optical Excitation and Detection of Vapor Bubbles around Plasmonic Nanoparticles. *Opt. Express* **2009**, *17*, 2538–2556.
29. Ramires, M. L. V.; Decastro, C. A. N.; Nagasaka, Y.; Nagashima, A.; Assael, M. J.; Wakeham, W. A. Standard Reference Data for the Thermal-Conductivity of Water. *J. Phys. Chem. Ref. Data* **1995**, *24*, 1377–1381.
30. Eastman, J. A.; Phillpot, S. R.; Choi, S. U. S.; Keblinski, P. Thermal Transport in Nanofluids. *Annu. Rev. Mater. Res.* **2004**, *34*, 219–246.
31. Oldenburg, S. J.; Averitt, R. D.; Westcott, S. L.; Halas, N. J. Nanoengineering of Optical Resonances. *J. Chem. Phys. Lett.* **1998**, *288*, 243–247.
32. Brinson, B.; Lassiter, J. B.; Levin, C. S.; Bardhan, R.; Mirin, N.; Halas, N. J. Nanoshells made easy: improving Au layer growth on nanoparticle surfaces. *Langmuir* **2008**, *24*, 14166–14171.
33. Duff, D. G.; Baiker, A.; Edwards, P. P. A New Hydrosol of Gold Clusters. 1. Formation and Particle Size Variation. *Langmuir* **1993**, *9*, 2301–2309.